Interface Passivation Effects on the Photovoltaic Performance of Quantum Dot Sensitized Inverse Opal TiO$_2$ Solar Cells

Kanae Hori [1], Yaohong Zhang [1,*] , Pimsiri Tusamalee [1,2], Naoki Nakazawa [1], Yasuha Yoshihara [1], Ruixiang Wang [3], Taro Toyoda [1], Shuzi Hayase [4] and Qing Shen [1,*]

[1] Department of Engineering Science, The University of Electro Communications, 1-5-1 Chofugaoka, Chofu, Tokyo 182-8585, Japan; hori@jupiter.pc.uec.ac.jp (K.H.); pimsiri.tsml@gmail.com (P.T.); nakazawa@jupiter.pc.uec.ac.jp (N.N.); yoshihara@jupiter.pc.uec.ac.jp (Y.Y.); toyoda@pc.uec.ac.jp (T.T.)

[2] Department of Physics, King Mongkut's Institute of Technology Ladkrabang, 1 Soi Chalongkrung 1, Ladkrabang, Bangkok 10520, Thailand

[3] Beijing Engineering Research Centre of Sustainable Energy and Buildings, Beijing University of Civil Engineering and Architecture, Beijing 102616, China; wangruixiang@bucea.edu.cn

[4] Graduate school of Life Science and Systems Engineering, Kyushu Institute of Technology, 2-4 Hibikino, Wakamatsu-ku, Kitakyushu, Fukuoka 808-0196, Japan; hayase@life.kyutech.ac.jp

*   Correspondence: yhzhang@jupiter.pc.uec.ac.jp (Y.Z.); shen@pc.uec.ac.jp (Q.S.); Tel.: +81-042-443-5471 (Q.S.)

check for updates

Abstract: Quantum dot (QD)-sensitized solar cells (QDSSCs) are expected to achieve higher energy conversion efficiency than traditional single-junction silicon solar cells due to the unique properties of QDs. An inverse opal (IO)-TiO$_2$ (IO-TiO$_2$) electrode is useful for QDSSCs because of its three-dimensional (3D) periodic nanostructures and better electrolyte penetration compared to the normal nanoparticles (NPs)-TiO$_2$ (NPs-TiO$_2$) electrode. We find that the open-circuit voltages V_{oc} of the QDSSCs with IO-TiO$_2$ electrodes are higher than those of QDSSCs with NPs-TiO$_2$ electrodes. One important strategy for enhancing photovoltaic conversion efficiency of QDSSCs with IO-TiO$_2$ electrodes is surface passivation of photoanodes using wide-bandgap semiconducting materials. In this study, we have proposed surface passivation on IO-TiO$_2$ with ZnS coating before QD deposition. The efficiency of QDSSCs with IO-TiO$_2$ electrodes is largely improved (from 0.74% to 1.33%) because of the enhancements of V_{oc} (from 0.65 V to 0.74 V) and fill factor (*FF*) (from 0.37 to 0.63). This result indicates that ZnS passivation can reduce the interfacial recombination at the IO-TiO$_2$/QDs and IO-TiO$_2$/electrolyte interfaces, for which two possible explanations can be considered. One is the decrease of recombination at IO-TiO$_2$/electrolyte interfaces, and the other one is the reduction of the back-electron injection from the TiO$_2$ electrode to QDs. All of the above results are effective for improving the photovoltaic properties of QDSSCs.

Keywords: quantum dot-sensitized solar cells (QDSSCs); inverse opal-TiO$_2$; surface passivation

1. Introduction

Renewable and low-cost energy is increasingly demanded which has created some remarkable research in the field of next-generation solar cells. Semiconductor quantum dot (QD)-sensitized solar cells (QDSSCs) have attracted much interest because they show some advantages compared to dye-sensitized solar cells [1–4]. QDs are beneficial because of their high optical absorption coefficients, multiple exciton generation, and large intrinsic dipole moments [4–6]. It has been expected that the maximum theoretical efficiency of QD-based solar cells would be 44% [7], which is much higher than that of traditional single-junction silicon solar cells (about 30%) [8].

The morphology of the TiO_2 electrodes is one main factor for the photovoltaic performance of the QDSSCs. In general, nanoparticles (NPs)-TiO_2 electrodes are employed in the QDSSCs because they have higher surface areas for adsorbing the QDs, and thus, photocurrents can be enhanced [9,10]. However, the disadvantage of NPs-TiO_2 electrodes is the low electron transport which results from the interfacial resistance and electron scattering in the NPs electrodes [11]. One dimensional (1D) nanofiber or whisker electrode, which can provide a direct pathway for charge transport, was usually employed in solar cells [12,13]. In addition to the 1D semiconducting oxides, the inverse opal (IO)-TiO_2 electrode has three dimensional (3D) periodic mesoporous nanostructures, which is also useful for the application of QDSSCs. This is because of the possible better electrolyte penetration in the IO-TiO_2 electrodes compared to the NPs-TiO_2 electrodes. In addition, the ordered 3D structure in the case of IO-TiO_2 electrodes is expected to be better for the electron transport in the TiO_2 electrode. It was observed that the open-circuit voltage (V_{oc}) of the CdSe QDSSCs with IO-TiO_2 electrodes was 0.2 V higher than that of the QDSSCs with the NPs-TiO_2 electrodes [14,15].

In QDSSCs, the interfacial recombination plays an important role in the performance of QDSSCs, especially in the V_{oc} of the device. As shown in Figure 1, there are usually three interfacial recombination paths occurring at the photoelectrode of QDSSCs, i.e., at the QDs/electrolyte interface (Rec 1), at the TiO_2/electrolyte interface (Rec 2), and at the TiO_2/QDs interface (Rec 3) [16–18]. One important strategy for reducing the recombination, thereby enhancing photovoltaic conversion efficiency of QDSSCs, is the surface passivation of the photoanode using wide-bandgap semiconducting materials. ZnS is commonly used as the surface passivation layer on QD-sensitized photoanodes [9,14,19,20]. ZnS passivation by the successive ionic layer adsorption and reaction (SILAR) method utilizes its advantage of straightforward preparation and striking enhancement of photovoltaic conversion efficiency. Diguna et al. applied CdSe QDSSCs on IO-TiO_2 electrodes, in which ZnS passivation was applied on the surfaces of CdSe QDs [14]. All of the photovoltaic performances were significantly improved. Hachiya et al. applied the ZnS passivation on the PbS QDs and studied the influences of the ZnS passivation on electron injection and charge recombination processes of the PbS QDSSCs [20]. Their results demonstrated that the ZnS passivation could greatly enhance the charge injection efficiency through the decrease in the carrier trapping and charge recombination (Rec 1 and Rec 2) after the ZnS passivation. However, in those works, the surface passivation of the photoanode by ZnS coating can only efficiently diminish the recombination occurring through the Rec 1 and Rec 2 paths in QDSSCs; thus, the recombination occurring at the TiO_2/QDs interface (Rec 3) also needs to be blocked. However, there are no reports on the surface passivation of IO-TiO_2 before the QDs deposition to date.
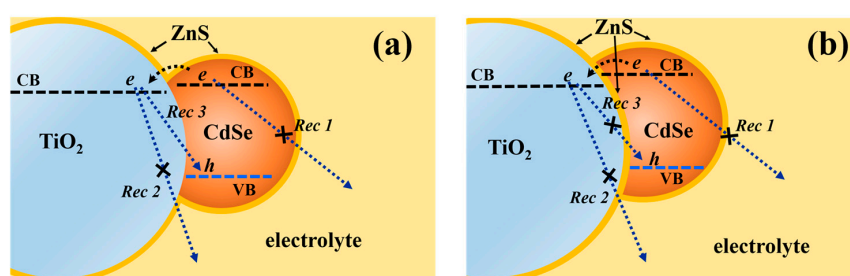

Figure 1. Schematic diagrams of interfacial recombination paths occurring at a photoelectrode. The ZnS coating deposited after the deposition of CdSe quantum dots (QDs) (**a**); and before and after the deposition of CdSe QDs (**b**).

In this study, we have proposed surface passivation on IO-TiO_2 with ZnS passivation before QD deposition. Effects of ZnS passivation cycles on the photovoltaic properties have been investigated systematically. Passivation at the interface between IO-TiO_2 and QDs with ZnS coating improved the fill factor (*FF*) and V_{oc} significantly because of the suppression of interfacial recombination,

which corresponded to an increase of the electron lifetime in the TiO_2 electrodes after the ZnS passivation.

2. Results and Discussion

We prepared four different types of samples, i.e., TiO_2, TiO_2/ZnS, TiO_2/CdSe QD/ZnS and TiO_2/ZnS/CdSe QD/ZnS samples. The former two were IO-TiO_2 electrodes with and without ZnS passivation on the electrodes. The latter two were CdSe QDs adsorbed on these IO-TiO_2 electrodes, and finally, ZnS (2 cycles) were adsorbed on the QD surfaces. The optical absorption properties of the prepared electrodes were investigated using the photoacoustic (PA) technique and the PA spectra are shown in Figure 2 and Figure S1. The PA spectra were normalized at the photon energy of 3.7 eV. The PA spectra of TiO_2 and TiO_2/ZnS were almost the same and no apparent shift was observed. This is because the bandgap energy of ZnS (3.6 eV) was higher than that of TiO_2 (3.2 eV). However, red shifts of the PA spectra were observed clearly after CdSe QD adsorption. Moreover, we found that the adsorption of the QD became faster in the case of the TiO_2 electrode with ZnS passivation layers. This phenomenon is considered to result from the possible formation of CdS between ZnS and CdSe QDs. Therefore, the samples with and without ZnS passivation adsorbed CdSe QDs for 4 h and 9 h, respectively, to make the QD size the same. The results are displayed in Figure 2. Here, the PA shoulder was assumed to be the first excitation energy level, E_1, of the CdSe QDs [9,21,22]. The average diameter of the QDs could be estimated by using the effective mass approximation [23,24], as shown in Equation (1):

$$\Delta E = E_1 - E_g = \frac{h^2}{8r^2}\left(\frac{1}{m_e} - \frac{1}{m_h}\right),\qquad(1)$$

where ΔE is the bandgap shift, E_g is the bandgap energy, r is the radius of the QDs, and m_e, m_h, and m_0 are the effective electron mass, hole mass, and electron rest mass, respectively ($m_e = 0.13\ m_0$, $m_h = 0.44\ m_0$, and $m_0 = 9.11 \times 10^{-31}$ kg [25]). By applying the value of E_1, the average diameter was estimated to be about 6.5 nm.
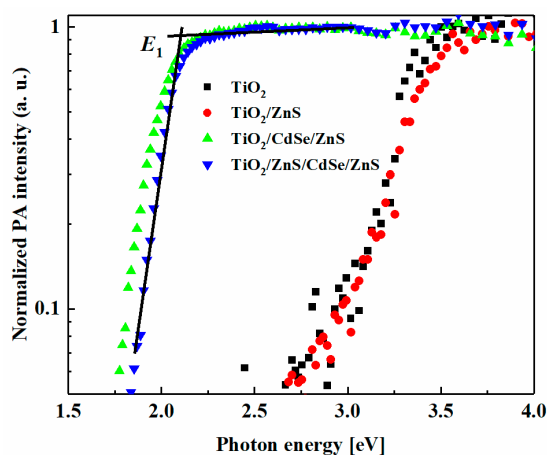

Figure 2. Normalized photoacoustic (PA) spectra of TiO_2, TiO_2/ZnS, TiO_2/CdSe QD/ZnS and TiO_2/ZnS/CdSe QD/ZnS.

Figures 3 and 4 show the typical scanning electron microscopy (SEM) images of the IO-TiO_2 without ZnS passivation (a), with 5 cycles of ZnS passivation (b) and with 15 cycles of ZnS passivation (c), without and with CdSe QD adsorption, respectively. As shown in Figure 3, the wall of the IO-TiO_2 electrode became thicker after ZnS passivation cycle increased. Figure 4 and Figure S2 show that CdSe QD formation initiated on the TiO_2 surface. A highly ordered TiO_2 framework with air holes was obtained after 5 cycles of ZnS passivation. However, at 15 cycles of ZnS passivation, the IO structure broke and its porous size became smaller after QD adsorption. The reason of the IO breakdown is the

washing of the electrodes during the SILAR process. In this method, dissolved cationic and anionic precursors are put into two beakers, and then the bare electrode is dipped alternatively into each solution for growing the QDs on the electrode. After absorption of Zn^{2+} or S^{2-} ion, the electrode needs to be washed with methanol. With the number of ZnS deposition cycles increasing, washing time is multiply increasing. Therefore, it is thought that the surfaces of some IO structures were destroyed.
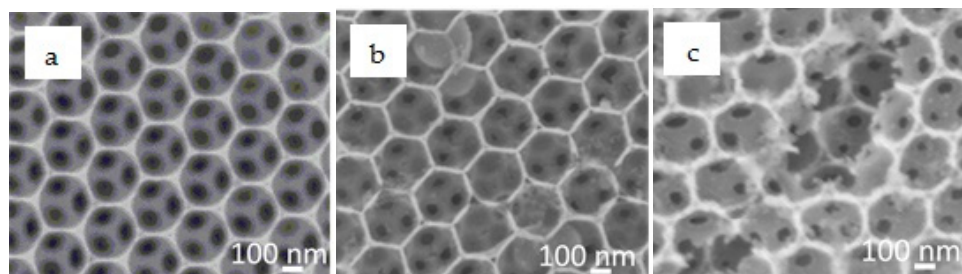

Figure 3. SEM images of inverse opal (IO)-TiO$_2$ without ZnS passivation (**a**); with 5 cycles of ZnS passivation (**b**); with 15 cycles of ZnS passivation (**c**).
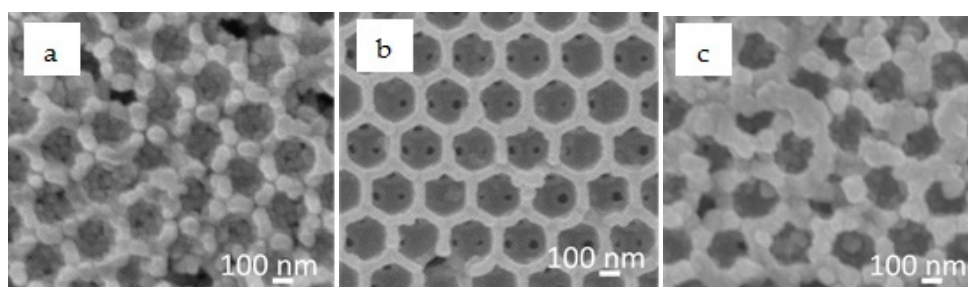

Figure 4. SEM images of CdSe QD deposited IO-TiO$_2$ without ZnS passivation (**a**); with 5 cycles of ZnS passivation (**b**); with 15 cycles of ZnS passivation (**c**).

Figure 5 shows the incident photon-to-current conversion efficiency (IPCE) spectra of the CdSe QDSSCs with different ZnS passivation layers. The IPCE peak value was about 24% at 550 nm for the device without ZnS passivation. For enhancing the IPCE values, it is necessary to prepare thicker IO-TiO$_2$ electrodes. As shown in Figure 5, the IPCE value decreased greatly as the ZnS passivation cycle number exceeded 10. This is because of the reduction of electron injection from CdSe QDs to IO-TiO$_2$ for thicker ZnS passivation layers.
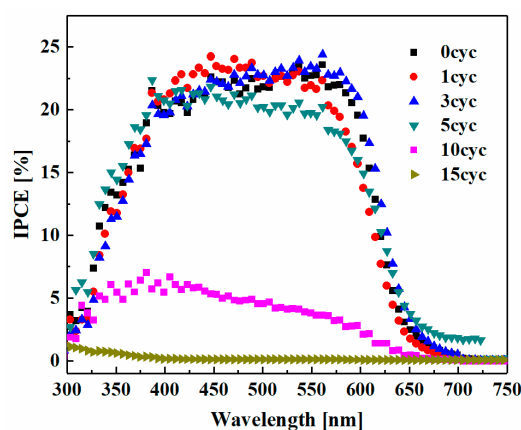

Figure 5. The incident photon-to-current conversion efficiency (IPCE) spectra for samples with different ZnS passivation layers.

To confirm the reduction of the electron injection for thicker ZnS passivation layers, transient absorption (TA) kinetics were detected for the CdSe QDs deposited on the IO-TiO$_2$ with and without ZnS passivation. Figure S3 shows the TA responses of the samples without and with 10-cycle ZnS passivation. The probe wavelength used here was 570 nm, which corresponds to the band-edge absorption of the CdSe QDs. Therefore, the TA decay mostly reflects the electron injection from the CdSe QDs to the IO-TiO$_2$. The TA response can be fitted using a bi-exponential function ($y = A_1\exp(-t/t_1) + A_2\exp(-t/t_2) + A_3)$), and Table S1 shows the least-squares best fit parameters. From Figure S3 and Table S1, we can clearly find that the TA decay became much slower in the case of the samples with a 10-cycle ZnS passivation layer between the IO-TiO$_2$ and the CdSe QDs. This result clearly indicated the reduction of electron injection from the CdSe QDs to IO-TiO$_2$ for thicker ZnS passivation layers.

The dependence of the photocurrent density–voltage (*J–V*) properties on the passivation cycles is shown in Figure 6. The short-circuit current density (J_{sc}), V_{oc}, *FF*, and the power conversion efficiency (η) value of solar cells determined from *J–V* curves are summarized in Table 1. As the ZnS passivation cycle number increased up to 5, the J_{sc} was almost unchanged, but V_{oc} and *FF* increased greatly. Then, as the ZnS passivation cycle number increased further, i.e., the 10 and 15 cycles, J_{sc} decreased significantly, which was consistent with the IPCE spectra. As a result, the solar cell with 5 cycles of ZnS passivation exhibited the highest η (1.33%). Compared to the cell without ZnS passivation, the presence of ZnS passivation layers significantly increased η by ~180%. V_{oc} and *FF* were also remarkably enhanced with the increased ZnS passivation cycle up to 5 cycles. This result suggested that the ZnS passivation could reduce the interfacial recombination at the IO-TiO$_2$/QDs and IO-TiO$_2$/electrolyte interfaces, for which two possible explanations can be considered. One is the decrease of recombination at the IO-TiO$_2$/electrolyte interface (Rec 2), and the other one is the reduction of the back-electron injection from the TiO$_2$ electrode to QDs (Rec 3). On the other hand, the great reduction of J_{sc} and IPCE values for 10 or more ZnS passivation cycles indicated that electron injection to TiO$_2$ became very difficult for thicker ZnS passivation layers.
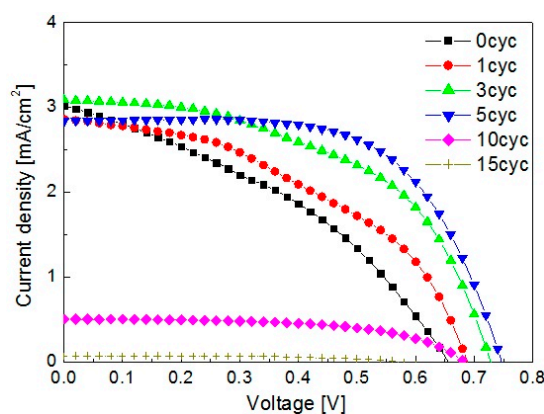

Figure 6. Photocurrent density–voltage *(J–V)* curves of CdSe quantum dot-sensitized solar cells (QDSSCs), where the IO-TiO$_2$ is treated with (from 1 cycle to 15 cycles) and without ZnS surface passivation (0 cycle).

Table 1. Dependence of the photovoltaic properties on the passivation cycles [a].

ZnS Cycle	J_{sc} [mA/cm^2]	V_{oc} [V]	*FF*	η [%]
0	3.0 ± 0.2	0.65 ± 0.01	0.37 ± 0.02	0.74 ± 0.02
1	2.9 ± 0.2	0.69 ± 0.02	0.44 ± 0.02	0.86 ± 0.05
3	3.1 ± 0.2	0.73 ± 0.01	0.52 ± 0.01	1.17 ± 0.03
5	2.8 ± 0.2	0.74 ± 0.01	0.63 ± 0.01	1.33 ± 0.03
10	0.5 ± 0.1	0.68 ± 0.02	0.58 ± 0.02	0.20 ± 0.04
15	0.1 ± 0.05	0.57 ± 0.03	0.57 ± 0.04	0.02 ± 0.01

[a] To account for experimental errors, four devices of each type are measured to give the reported averages and deviations. The active area of each device is 0.28 cm^2.

In order to reveal the effects of ZnS coating on charge carrier recombination and charge carrier lifetime in these QDSSCs, transient open-circuit voltage decay measurements (OCVD) were carried out. Figure S4 shows the OCVD curves of the IO-TiO$_2$/CdSe QDSSCs, where the IO-TiO$_2$ electrode was passivated with and without ZnS. The decay of V_{oc} in the solar cells became slower with the increased ZnS passivation cycles. The effective electron lifetime (τ) from the decay of V_{oc} can be determined by Equation (2) as follows [26,27]:

$$\tau = \frac{k_B T}{e}\left(\frac{dV_{OC}}{dt}\right)^{-1} \tag{2}$$

where e is the elementary charge, k_B is the Boltzmann constant and T is temperature. Figure 7 shows τ of CdSe QD-sensitized IO-TiO$_2$ solar cells with different ZnS passivation cycles, which was calculated from the V_{oc} decay curves (Figure S4). From Figure 7, we can clearly see that τ of these QDSSCs with ZnS passivation layers was longer than that of device without ZnS passivation layers, especially at the high V_{oc} region. In addition, with the ZnS passivation cycle number increasing, the value of τ became larger at the same voltage. Larger τ reflected that there was less recombination in the devices. It means that both of recombination occurring at the IO-TiO$_2$/electrolyte interface and the IO-TiO$_2$/CdSe QDs interface were suppressed after ZnS coating. Notably, for 10-cycle and 15-cycle samples, although there was less recombination in these two type devices compared with the other four samples, the electron injection from CdSe QDs to IO-TiO$_2$ became difficult due to the thicker ZnS layers, which resulted in low J_{sc} and efficiency. This result agreed strongly with the photovoltaic performance, as shown in Figure 6 and Table 1.
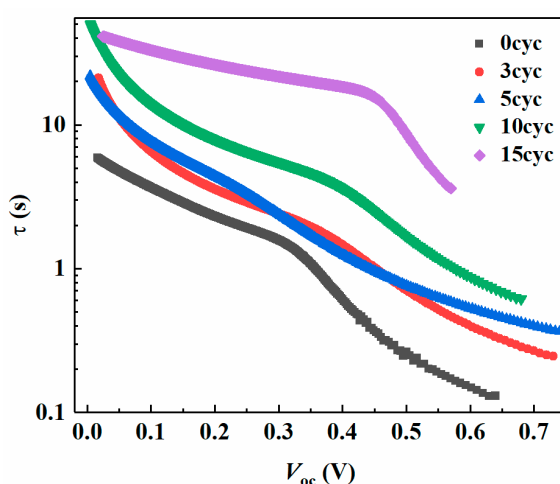

Figure 7. Effective electron lifetime curves of the IO-TiO$_2$/CdSe QDSSCs, of which the IO-TiO$_2$ electrodes were passivated with (from 1 cycle to 15 cycles) and without ZnS.

To clarify the mechanism of the ZnS passivation on the increase of the electron lifetime in the QDSSCs, impedance spectroscopy characterization was carried out. The results are shown in Figure S5. There was a large difference between the impedance spectra of the QDSSCs with and without ZnS passivation. Then, the recombination resistances, R_{rec}, of the QDSSCs were obtained by fitting the impedance spectra (Figure S5a) with an equivalent circuit, according to the method reported by Bisquert and co-workers [28]. The ZnS passivation has a great effect on the R_{rec} and increased the R_{rec} greatly, as shown in Figure S5b. R_{rec} was reversely proportional to the recombination rate in the QDSSCs. The ZnS passivation on the IO-TiO$_2$ electrodes decreased the recombination of the injected electrons in TiO$_2$ to the holes remained in the CdSe QDs and/or to the accepting species in the electrolyte. Thus, as a result, V_{oc} and FF of the resultant QDSSCs were enhanced. This result is in good consistency with the OCVD results as mentioned above.

3. Materials and Methods

3.1. Preparation

The IO-TiO_2 films were prepared on fluorine-doped tin oxide (FTO) coated glass by filling the void in an artificial template and subsequently removing the template [29,30]. Uniform polystyrene (PS) latex (the diameter was 474 nm) suspensions were dispersed ultrasonically for 30 min to break down the aggregated particles. The fabricated opal templates were prepared by vertically immersing the FTO substrate in a 0.1 wt.% PS suspension and fully evaporating the solvent in an oven at 40 °C for 1 to 2 days [29]. Subsequently, the substrate was immersed into a TiO_2 precursor sol with a mixture of absolute ethanol, hydrochloric acid, tetrabutyl titanate, and deionized water to ensure the filling of all the voids for 10 min [30]. Finally, the substrate was annealed at 450 °C for 3 h in air with a ramp rate of 1 °C/min to remove the PS opal template. For the ZnS passivation on the IO-TiO_2 surface, the SILAR method was used [19]. The IO-TiO_2 electrode was immersed alternately in the $Zn(CH_3COO)_2$ solution (0.1 M in methanol) and the Na_2S solution (0.1 M in pure water and methanol mixed solvent (1:1 by volume)) for 1 min. The processes were repeated several times (0, 1, 3, 5, 10, 15 cycles). After the ZnS passivation, the adsorption of CdSe QDs on IO-TiO_2 was conducted at 10 °C by a chemical deposition method [31]. First, the Na_2SeSO_3 aqueous solution is prepared by stirring elemental Se powder in an aqueous solution of 200 mM Na_2SO_3 at 70 °C for about 6 h. Then, 80 mM $CdSO_4$ and 120 mM $N(CH_2COONa)_3$ were mixed with an 80 mM Na_2SeSO_3 solution. The samples were immersed in the final chemical solution at 10 °C to promote the absorption of CdSe QDs and kept in the dark for some time (9 h for the sample without ZnS passivation and 4 h for those with ZnS passivation). After CdSe QD adsorption, the electrodes were passivated by ZnS using the SILAR method by 2 cycles to decrease the surface defects of the QD surfaces [9]. The thickness of the active layers (IO-TiO_2/CdSe QD) without and with ZnS passivation on the IO-TiO_2 was almost the same (about 6.5 µm), which were determined by the cross-sectional SEM images (Figure S6).

3.2. Measurement

The optical absorptions of the prepared electrodes were investigated using the PA technique [20]. The PA spectra were measured within the wavelength range between 300 and 800 nm at room temperature. The morphologies of samples were investigated with SEM (JSM-6340, JEOL, Japan) and TEM (JEM-2100F, JEOL, Japan). Sandwiched solar cells were assembled by using a CdSe QD-sensitized IO-TiO_2 photoanode and a Cu_2S counter electrode to measure the *J–V* characteristics, the IPCE spectra and the OCVD. A polysulfide solution was used as an electrolyte with the S and Na_2S concentrations of 1 M [32,33]. The IPCE spectra were measured using a homemade equipment within the wavelength range between 300 and 800 nm. The *J–V* characteristics were measured using a solar simulator (Peccell Technologies, Inc., Yokohama, Japan) with 100 mW/cm^2 under A.M. 1.5. The TA spectra were measured using a titanium/sapphire laser (CPA-2010, Clark-MXR, Inc., Dexter, MI, USA) with a repetition rate of 1 kHz and a pulse width of 150 fs. The wavelengths of the pump and probe light were 470 nm and 570 nm, respectively. The OCVD measurements were carried out using a 405 nm laser diode. The voltage decay from the device was recorded using a digital oscilloscope (DS-5554, Iwatsu, Japan). Electrochemical impedance spectra were measured under dark conditions using an impedance analyzer (SP-300, BioLogic, Seyssinet-Pariset, France), where a small voltage perturbation (10 mV rms) was applied at frequencies from 1 MHz to 0.1 Hz for different forward-biased voltages.

4. Conclusions

We have studied the effects of the passivation at the interface between IO-TiO_2 and QDs with ZnS coating on the photovoltaic properties and its mechanism. V_{OC} and *FF* have been improved to be as high as 0.74 V and 0.63, respectively, with 5 cycles of ZnS passivation. The efficiency of QDSSCs with IO-TiO_2 electrodes was greatly improved (about 180%) after 5 cycles of ZnS passivation. The electron lifetime was enhanced significantly with the increased ZnS passivation cycle. However, excess ZnS

passivation reduced electron injection from the QDs to the TiO_2 for thicker ZnS passivation layers and worse penetration of electrolyte occurred due to the broken IO-TiO_2 structure. In order to improve the photovoltaic properties of QDSSC with IO-TiO_2 electrodes, it is needed to thicken TiO_2 and optimize the passivation material and thickness. This work would shed light on the investigation of other multi-junction solar cells, such as perovskite solar cells.

Supplementary Materials: The following are available online at http://www.mdpi.com/2079-4991/8/7/460/s1, Figure S1: PA spectra of CdSe sensitized IO-TiO_2 with and without ZnS passivation, Figure S2: TEM images of IO-TiO_2, IO-TiO_2/ZnS and IO-TiO_2/ZnS/CdSe QD/ZnS, Figure S3: TA responses for the CdSe QD deposited IO-TiO_2 with and without ZnS passivation, Figure S4: OCVD curves of IO-TiO_2/CdSe QDSSCs, Figure S5: Impedance spectra of CdSe QDSSCs with and without ZnS passivation, Figure S6: Cross sectional SEM images of CdSe QD deposited IO-TiO_2 with and without ZnS passivation, Table S1: Fitting result of Figure S3.

References

1. Shen, Q.; Arae, D.; Toyoda, T. Photosensitization of nanostructured TiO_2 with CdSe quantum dots: Effects of microstructure and electron transport in TiO_2 substrates. *J. Photochem. Photobiol. A Chem.* **2004**, *164*, 75–80. [CrossRef]

2. Mora-Seró, I.; Giménez, S.; Fabregat-Santiago, F.; Gómez, R.; Shen, Q.; Toyoda, T.; Bisquert, J. Recombination in quantum dot sensitized solar cells. *Acc. Chem. Res.* **2009**, *42*, 1848–1857. [CrossRef] [PubMed]

3. Toyoda, T.; Onishi, Y.; Katayama, K.; Sawada, T.; Hayase, S.; Shen, Q. Photovoltaics and photoexcited carrier dynamics of double-layered CdS/CdSe quantum dot-sensitized solar cells. *J. Mater. Sci. Eng. A B* **2013**, *3*, 601–608.

4. Sogabe, T.; Shen, Q.; Yamaguchi, K. Recent progress on quantum dot solar cells: A review. *J. Photonics Energy* **2016**, *6*, 040901. [CrossRef]

5. Nozik, A. Quantum dot solar cells. *Physica E* **2002**, *14*, 115–120. [CrossRef]

6. Bang, J.; Kamat, P. Quantum dot sensitized solar cells. A tale of two semiconductor nanocrystals: CdSe and CdTe. *ACS Nano* **2009**, *3*, 1467. [CrossRef] [PubMed]

7. Hanna, M.; Nozik, A. Solar conversion efficiency of photovoltaic and photoelectrolysis cells with carrier multiplication absorbers. *J. Appl. Phys.* **2006**, *100*, 074510. [CrossRef]

8. Shockley, W.; Queisser, H. Detailed balance limit of efficiency of pn junction solar cells. *J. Appl. Phys.* **1961**, *32*, 510–519. [CrossRef]

9. Shen, Q.; Kobayashi, J.; Diguna, L.J.; Toyoda, T. Effect of ZnS coating on the photovoltaic properties of CdSe quantum dot-sensitized solar cells. *J. Appl. Phys.* **2008**, *103*, 084304. [CrossRef]

10. Toyoda, T.; Oshikane, K.; Li, D.; Luo, Y.; Meng, Q.; Shen, Q. Photoacoustic and photoelectrochemical current spectra of combined CdS/CdSe quantum dots adsorbed on nanostructured TiO_2 electrodes, together with photovoltaic characteristics. *J. Appl. Phys.* **2010**, *108*, 114304. [CrossRef]

11. Benkstein, K.; Kopidakis, N.; Lagemaat, J.; Frank, A. Influence of the percolation network geometry on electron transport in dye-sensitized titanium dioxide solar cells. *J. Phys. Chem. B* **2003**, *107*, 7759–7767. [CrossRef]

12. Batmunkh, M.; Macdonald, T.; Shearer, C.; Bat-Erdene, M.; Wang, Y.; Biggs, M.; Parkin, I.; Nann, T.; Shapter, J. Carbon nanotubes in TiO_2 nanofiber photoelectrodes for high-performance perovskite solar cells. *Adv. Sci.* **2017**, *4*, 1600504. [CrossRef] [PubMed]

13. Gao, G.; Yu, L.; Vinu, A.; Shapter, J.; Batmunkh, M.; Shearer, C.; Yin, T.; Huang, P.; Cui, D. Synthesis of ultra-long hierarchical ZnO whiskers in a hydrothermal system for dye-sensitized solar cells. *RSC Adv.* **2016**, *6*, 109406–109413. [CrossRef]

14. Diguna, L.J.; Shen, Q.; Kobayashi, J.; Toyoda, T. High efficiency of CdSe quantum-dot-sensitized TiO$_2$ inverse opal solar cells. *Appl. Phys. Lett.* **2007**, *91*, 023116. [CrossRef]

15. Toyoda, T.; Yindeesuk, W.; Okuno, T.; Akimoto, M.; Kamiyama, K.; Hayase, S.; Shen, Q. Electronic structures of two types of TiO$_2$ electrodes: Inverse opal and nanoparticulate cases. *RSC Adv.* **2015**, *5*, 49623–49632. [CrossRef]

16. Tung, H.; Thao, N.; Vinh, L. The reduced recombination and the enhanced lifetime of excited electron in QDSSCs based on different ZnS and SiO$_2$ passivation. *Int. J. Photoenergy* **2018**, 8545207. [CrossRef]

17. Huang, F.; Zhang, L.; Zhang, Q.; Hou, J.; Wang, H.; Wang, H.; Peng, S.; Liu, J.; Cao, G. High efficiency CdS/CdSe quantum dot sensitized solar cells with two ZnSe layers. *ACS Appl. Mater. Interfaces* **2016**, *8*, 34482–34489. [CrossRef] [PubMed]

18. Zhang, Y.; Zhu, J.; Yu, X.; Wei, J.; Hu, L.; Dai, S. The optical and electrochemical properties of CdS/CdSe co-sensitized TiO$_2$ solar cells prepared by successive ionic layer adsorption and reaction processes. *Sol. Energy* **2012**, *86*, 964–971. [CrossRef]

19. Yang, S.M.; Huang, C.H.; Zhai, J.; Wang, Z.S.; Liang, L. High photostability and quantum yield of nanoporous TiO$_2$ thin film electrodes co-sensitized with capped sulfides. *J. Mater. Chem.* **2002**, *12*, 1459–1464. [CrossRef]

20. Hachiya, S.; Shen, Q.; Toyoda, T. Effect of ZnS coatings on the enhancement of the photovoltaic properties of PbS quantum dot-sensitized solar cells. *J. Appl. Phys.* **2012**, *111*, 104315. [CrossRef]

21. Rosencwaig, A. Photoacoustic spectroscopy of solids. *Phys. Today* **1975**, *28*, 23–30. [CrossRef]

22. Shen, Q.; Toyoda, T. Characterization of nanostructured TiO$_2$ electrodes sensitized with CdSe quantum dots using photoacoustic and photoelectrochemical current methods. *Jpn. J. Appl. Phys.* **2004**, *43*, 2946–2951. [CrossRef]

23. Ekimov, A.I.; Efros, A.L.; Onushchenko, A.A. Quantum size effect in semiconductor microcrystals. *Solid State Commun.* **1985**, *56*, 921–924. [CrossRef]

24. Bawendi, M.G.; Kortan, A.R.; Steigerwald, M.L.; Brus, L.E. X-ray structural characterization of larger CdSe semiconductor clusters. *J. Chem. Phys.* **1989**, *91*, 7282–7290. [CrossRef]

25. Nomura, S.; Kobayashi, T. Nonparabolicity of the conduction band in CdSe and CdS$_x$Se$_{1-x}$ semiconductor microcrystallites. *Solid State Commun.* **1991**, *78*, 677–680. [CrossRef]

26. Zaban, A.; Greenshtein, M.; Bisquert, J. Determination of the electron lifetime in nanocrystalline dye solar cells by open-circuit voltage decay measurements. *Chem. Phys. Chem.* **2003**, *4*, 859–864. [CrossRef] [PubMed]

27. Zhang, Y.; Wu, G.; Mora-Seró, I.; Ding, C.; Liu, F.; Huang, Q.; Ogomi, Y.; Hayase, S.; Toyoda, T.; Wang, R.; et al. Improvement of photovoltaic performance of colloidal quantum dot solar cells using organic small molecule as hole-selective layer. *J. Phys. Chem. Lett.* **2017**, *8*, 2163–2169. [CrossRef] [PubMed]

28. González-Pedro, V.; Xu, X.; Mora-Seró, I.; Bisquert, J. Modeling high-efficiency quantum dot sensitized solar cells. *ACS Nano* **2010**, *4*, 5783–5790. [CrossRef] [PubMed]

29. Diguna, L.J.; Murakami, M.; Sato, A.; Kumagai, Y.; Ishihara, T.; Kobayashi, N.; Shen, Q.; Toyoda, T. Photoacoustic and photoelectrochemical characterization of inverse opal TiO$_2$ sensitized with CdSe quantum dots. *Jpn. J. Appl. Phys.* **2006**, *45*, 5563–5568. [CrossRef]

30. Zhang, X.; Liu, Y.; Lee, S.; Yang, S.; Kang, Z. Coupling surface plasmon resonance of gold nanoparticles with slow-photon-effect of TiO$_2$ photonic crystals for synergistically enhanced photoelectrochemical water splitting. *Energy Environ. Sci.* **2014**, *7*, 1409–1419. [CrossRef]

31. Gorer, S.; Hodes, G. Quantum size effects in the study of chemical solution deposition mechanisms of semiconductor films. *J. Phys. Chem.* **1994**, *98*, 5338–5346. [CrossRef]

32. Niitsoo, O.; Sarkar, S.K.; Pejoux, C.; Ruhle, S.; Cahen, D.; Hodes, G. Chemical bath deposited CdS/CdSe-sensitized porous TiO$_2$ solar cells. *J. Photochem. Photobiol. A* **2006**, *181*, 306–313. [CrossRef]

33. Shen, Q.; Yamada, A.; Tamura, S.; Toyoda, T. CdSe quantum dot-sensitized solar cell employing TiO$_2$ nanotube working-electrode and Cu$_2$S counter-electrode. *Appl. Phys. Lett.* **2010**, *97*, 123107. [CrossRef]